Three dimensional OCT images from retina and skin

Adrian Gh. Podoleanu, John A. Rogers, David A. Jackson,
Applied Optics Group, School of Physical Sciences, University of Kent, Canterbury, CT2 7NR, UK
http://www.ukc.ac.uk/physical-sciences/aog/Low Cohe/

Shane Dunne
Ophthalmic Technologies, Inc., Toronto, Canada
http://www.oti-canada.com/

Abstract: We demonstrate the functionality of an en-face optical coherence tomography (OCT) system with images from the retina and skin. En-face images collected at different depths are subsequently used to reconstruct a 3D volume of the tissue. The reconstruction allows software inferred OCT longitudinal images at any transversal position in the stack. The position in depth in the stack before creating longitudinal OCT images is also adjustable, offering a valuable guidance tool for exploring the 3D volume of the tissue. This is illustrated by Quick time movies showing either depth or lateral exploration along one of two possible different directions in the stack of transversal OCT images. Sufficient accuracy of the volume rendered is obtained in 20 seconds when the system operates at 2 frames a second. The system, equipped with the 3D rendering feature acts as a valuable diagnostic tool allowing "peeling off" of transversal and longitudinal biologic material to investigate different internal features.

OCIS codes: (170.4500) Optical coherence tomography; (170.3880) Medical and biological Imaging; (120.3890) Medical optics instrumentation.

References and links

1. R. C. Youngquist, S. Carr, and D. E. N. Davies, "Optical coherence-domain reflectometry: A New Optical Evaluation Technique," Opt. Lett. **12,** 158-160 (1987).
2. D. Huang, E.A. Swanson, C. P. Lin, J. S. Schuman, W. G. Stinson, W. Chang, M. R. Hee, T. Flotte, K. Gregory, C. A. Puliafito and J. G. Fujimoto, "Optical coherence tomography," Science, **254** 1178-1181 (1991).
3. C. Puliafito, *Optical coherence tomography of ocular diseases*, (Thorofare, NJ, SLACK Inc., 1996).
4. J. M. Schmitt, M. J. Yadlowsky, R. F. Bonner, "Subsurface imaging of living skin with optical coherence microscopy," Dermatology, **191,** 93-98 (1995).
5. A. Pagnoni, A. Knuettel, P. Welker, M. Rist, T. Stoudemayer, L. Kolbe, I. Sadiq and A. M. Kligman, "Optical coherence tomography in dermatology," Skin Research and Technology, **5,** 83-87 (1995).
6. A. E. Elsner, L. Moraes, E. Beausencourt, A. Remky, S.A. Burns, J. J. Weiter, J. P. Walker, G. L. Wing, P. A. Raskauskas and L. M. Kelly, "Scanning laser reflectometry of retinal and subretinal tissues," Opt. Express, **6**, 243-250 (2000), http://www.opticsexpress.org/oearchive/source/21766.htm.
7. A. Gh. Podoleanu, M. Seeger, G. M. Dobre, D. J. Webb, D. A. Jackson and F. Fitzke "Transversal and longitudinal images from the retina of the living eye using low coherence reflectometry," J. Biomed Optics, **3,** 12-20 (1998).
8. C. K. Hitzenberger, A. Baumgartner, A. F. Fercher, "Dispersion induced multiple signal peak splitting in partial coherence interferometry," Opt. Commun., **154**, 179-185 (1998).
9. A. Gh. Podoleanu, G. M. Dobre, D. J. Webb, D. A. Jackson, 'Coherence imaging by use of a Newton rings sampling function', *Opt. Lett.* **21**, 1789-1791 (1996).
10. A. Gh. Podoleanu, G. M. Dobre and D. A. Jackson, "En-face coherence imaging using galvanometer scanner modulation," *Opt. Lett*., **23**, 147-149 (1998).
11. B. Hoeling, A. Fernandez, R. Haskell, E. Huang, W. Myers, D. Petersen, S. Ungersma, R. Wang, M. Williams and S. Fraser, "An optical coherence microscope for 3-dimensional imaging in developmental biology ", **6**, Opt. Express, 136-145 (2000), http://epubs.osa.org/oearchive/source/19250.htm.
12. Y. Pan and D. Farkas, "Non-invasive Imaging of Living Human Skin with Dual-wavelength Optical Coherence Tomography in Two and Three Dimensions," J. Biomed Optics, **3**, 446-455 (1998).

#23434 - $15.00 US Received September 03, 2000; Revised October 12, 2000

13. S.A. Boppart, G.J. Tearney, B.E. Bouma, J.F. Southern, M.E. Brezinski, and J.G. Fujimoto, "Noninvasive assessment of the developing *Xenopus* cardiovascular system using optical coherence tomography," Proc. Natl. Acad. Sci. **94**, 4256-4261 (1997).
14. J. Barton, J.A. Izatt, M.D. Kulkarni, S. Yazdanfar, A.J. Welch, "Three-Dimensional Reconstruction of Blood Vessels from in vivo Color Doppler Optical Coherence Tomography Images," Clinical and Laboratory Investigations Dermatology, **198**, 355-361 (1999).
15. L. Giniunas, R. Danielius, Karkockas, "Scanning delay line with a rotating-parallelogram prism for low-coherence interferometry," Appl. Opt., **38**,. 7076-7079 (1999).
16. A. M. Rollins, M. D. Kulkarni, S. Yazdanfar, R. Ungarunyawee and J. A. Izatt, "In vivo video rate optical coherence tomography," Opt. Express, **3**, No.6, 219-229 (1998), http://epubs.osa.org/oearchive/source/5873.htm
17. A. Gh.Podoleanu, J. A. Rogers, D. A. Jackson, "OCT *En-face* Images from the retina with adjustable depth resolution in real time," IEEE Journal of Selected Topics in Quantum Electron., **5**, 1176-1184, (1999).
18. R. Rajadhyaksha, R. Anderson and R. Webb, "Video-rate confocal scanning laser microscope for imaging human tissues in vivo," Appl. Opt., **38**, 2105-2115 (1999).
19. A. Gh. Podoleanu and D. A. Jackson, "Noise Analysis of a combined optical coherence tomography and confocal scanning ophthalmoscope," Appl. Opt., **38**, 2116-2127 (1999).
20. A. Gh. Podoleanu, "Unbalanced versus balanced operation in an OCT system," Appl. Opt., **39**, 173-182 (2000).
21. B. R. Masters, "Three-dimensional confocal microscopy of the human optic nerve in vivo," Opt. Express, **3**, 356-359 (1998), http://epubs.osa.org/oearchive/source/6295.htm
22. Web page of the New York Eye and Ear infirmery: http://www.nyee.edu/glaucoma/octdata.htm.

1. Introduction

There is a growing interest in the use of OCT [1,2] by vision scientists and research ophthalmologists [3] as the increased depth resolution of the OCT promises to provide information on structures of the eye not discernible with a state of the art scanning laser ophthalmoscope (SLO). Also, OCT images from skin have been reported [4] showing detailed morphology and effects of drugs on the skin [5].

However, the majority of the reports [1-5] relate to the production of longitudinal OCT slices in the tissue, i.e. images containing the optical axis. This way of "cutting out" the tissue was stimulated mainly by a technical reason: when moving the mirror in the reference path, not only is the depth scanned, but a carrier is also produced. The carrier frequency is the Doppler shift produced by the longitudinal scanner itself (moving along the axis of the system, Z, to explore the tissue in depth). The image bandwidth, given by the speed the depth pixel size is scanned, appears in the spectrum of the photodetected signal as an enlargement of the Doppler frequency component.

It is also desirable to offer en-face images in real time, i.e. slices of the tissue at orientations perpendicular to the optic axis. For studies of the eye, this is extremely important. The SLO technology offers transversal images of the fundus [6] and a large data base of SLO images exist. The SLO expertise in recognizing ailments of the eye could be better transferred to the OCT technology if the images were of the same orientation.

This may also be valid for the skin, where transversal patterns of collagen or anisotropy may be of interest for diagnostic.

Obviously, transversal orientations may also be accessible using the conventional longitudinal OCT procedure if a sufficiently large number of images are collected at different transversal positions followed by software processing. However, this takes time and movements of the object between different slices may jeopardize the quality of the image being inferred.

If en-face (transversal) images [7] at a fixed depth are necessary, a path imbalance modulator is needed in order to create a carrier for the image bandwidth. This will obviously require the introduction of a phase modulator in one of the arms of the interferometer. This raises a couple of issues. There are low frequency phase modulators, using piezo or electrostrictive elements which can be used to stretch a short length of fiber up to a maximum frequency of $\approx$100 kHz. Their advantage is that they do not introduce either attenuation, dispersion or birefringence in the OCT set-up. However, if en-face fast imaging is required,

#23434 - $15.00 US Received September 03, 2000; Revised October 12, 2000

the image bandwidth necessary for instance to produce a frame of 3 mm x 3 mm in 1 Hz from the retina is greater than 100 kHz [7]. For larger bandwidth, very fast electro-optic phase modulators are known. However, the dispersion [8] and birefringence related effects may reduce the S/N ratio and distort the depth sectioning capabilities. This is why the introduction of a new component in the interferometer arms is undesirable and if possible, should be avoided.

We have shown [7,9,10] that the X or Y-scanning device itself introduces a path modulation which plays a similar role to the path modulation created by the longitudinal scanner in longitudinal imaging OCT set-ups. Theoretical analysis has shown that the OCT image production can be interpreted as interrogating the object with a specific sampling function. Depending on the position of the incident beam on the galvo-scanner mirror and on the interface optics used, the sampling function could look either as Newton rings [9] or as a regular grid of lines [10]. The sampling function is in fact a fringe pattern in transversal section. Consequently, when the beam scans the target, the OCT signal is modulated by this fringe pattern. As the pattern is not regular, the transversal resolution varies across the target and different frequencies result in contrast to OCT longitudinal imaging case where the carrier frequency is constant. A phase modulator at a frequency much larger than the signal bandwidth is desirable to insure a constant transversal resolution over the target. However, we have shown in [7] that for sufficient image size, the errors introduced in the image by the variable sampling pattern can be neglected. This was determined by comparing the effect of the external phase modulation with the effect of the galvo-scanning modulation. For an image size larger than 1 mm the external phase modulator has had little effect. Subsequently, we demonstrated OCT images of single layer objects using the modulation introduced by the galvanometer scanner only [10].

In the present paper we demonstrate that images from multi-layer objects can be generated using the same concept.

2. Different scanning procedures

An OCT system is generally based on a two beam interferometer. To obtain 3D information about the object, the OCT system is equipped with two scanning means, one to scan the object in depth and another one to scan the object transversally. Depending on the order these scanners are operated and on the scanning direction associated with the line displayed in the raster of the final image delivered, different possibilities exist. The majority of reports in literature [1-5,8] refer to the longitudinal imaging procedure as shown at the top of Fig. 1, where the lines in the image correspond to A-scans (the lines are along the depth coordinate)

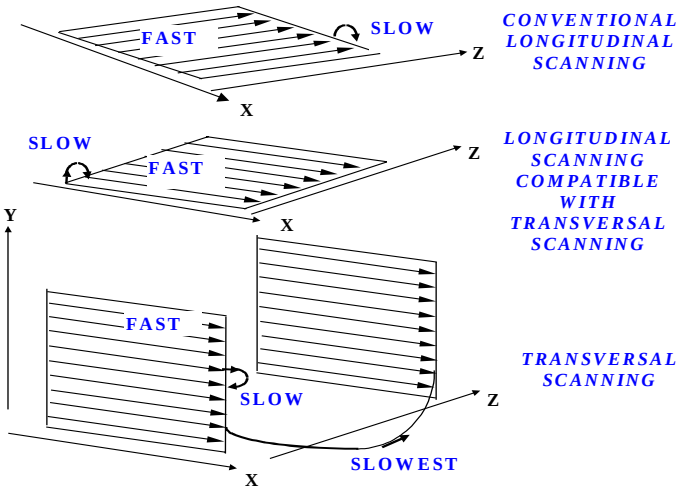

Figure 1. Three modes of operation of the three scanners in an OCT system.

#23434 - $15.00 US
Received September 03, 2000; Revised October 12, 2000

and the transversal scanner (along X or Y, with X shown in Fig.1) advances at a slower pace to build a B-scan image. We reversed this in our system, where the transversal scanner produces the fast lines in the image [7,9,10] and the longitudinal scanner advances slower, as shown in the middle of Fig. 1. This allows the production of OCT transversal images [7,9,10,11] for a fixed reference path, as illustrated in Fig. 1 bottom. One of the transversal scanner scans the object along the lines in the displayed image (X), the other transversal scanner advances a second co-ordinate (Y) in the transversal plane at a slower rate. Different transversal slices are collected for different depths Z, either by advancing the optical path difference in steps after each complete transversal XY scan or continuously at a speed for which the depth position of the point in the top left corner of the image and the depth position in the bottom right corner of the image do not differ by more than half the depth resolution. This provides the fastest pace for a continuous advancement of the scanner in depth.

3. Collecting 3D data

3D complete information could be collected in different ways, either acquiring many longitudinal OCT images at different en-face positions [12-14] or many en-face OCT images at different depth positions as shown in [11] and in the present paper. In principle, the volume rendered by either procedure from the tissue should be equivalent. However, the devices used to scan the object in the three directions are not identical. They are dedicated to either transversal OCT (fast galvanometer scanners [7,9,10, polygon mirrors [6] along with slow axial scanners) or to longitudinal OCT (turbine driven mirror [15] or fast axial scanners using diffraction grating [16] along with lower speed transversal scanners). This dedicated design determines the way the 3D information is collected.

For retina imaging we considered it more useful to have a transversal aspect of the image to insure compatibility of the OCT image with the aspect of the images generated by SLOs [6], as discussed in previous publications [7,17].

In the present paper we demonstrate 3D volume rendering from the eye in vivo using transversal OCT images collected at different depth. We use the same system to generate similar images from skin. Confocal images of skin which is a highly scattering tissue have recently been reported in vivo [18]. Consequently, our instrument could prove valuable not only for insuring compatibility with SLO images in the case of the eye [6] but for insuring compatibility with confocal imagers of the skin as well.

3.1. Configuration

The optical configuration is similar to that presented in [7], the low coherence source being a Superlum SLD at 860 nm. Using a plane mirror in the object arm and no transversal scanning, the FWHM of the depth sampling interval was 22 μm. The depth sampling interval in tissue is obtained by dividing this value by the index of refraction (this varies depending on the tissue, however a value of 1.4 can be used as a good approximation). In order to image different objects, adjustable interface optics were designed.

In the images presented below, no other phase modulation was employed apart from that introduced by the X-galvanometer scanner, in contrast to [11] where en-face imaging and 3D rendering relied entirely on the phase modulation introduced by a small plane mirror vibrated at f=125 kHz. The utilization of the modulator was made possible by a sufficiently low bandwidth in comparison with f, (due to a low scanning speed, a frame was obtained in 5 minutes). In our case, due to the relatively large image size and scanning rate, the bandwidth is larger and such a simple modulator cannot be employed. In [7] we have demonstrated the role played by the image size in balancing the effects of an external phase modulator and of the modulation produced by the transversal scanner. For instance, when the image size was three times smaller than that used here, it was advantageous to employ a phase modulator working at f=30 kHz

As disadvantage is that without external fixed modulation, the procedure of adding the squared components of the photodetected signal at odd and even multiples of frequency f

#23434 - $15.00 US Received September 03, 2000; Revised October 12, 2000

cannot be implemented any more. Such procedure was implemented in [7] and [11] to reduce the effect of vibrational noise and thermal fluctuation.

Because no external modulator is employed here, the electronic receiver after the photodetector was simplified and instead of two channels on 2f and 3f [7] we used only one amplifier with a bandwidth of 125 kHz. Following the analysis in references [19, 20], the minimum reflectivity measurable with the system for a 125 kHz bandwidth and 140 μW power to the object was $R \approx 3x10^{-8}$ with a S/N = 9. The signal S is evaluated as the electrical power of the OCT signal and N as the electrical power noise (an explanation for the coefficient 9 used in imaging situations is given in [19]). The transversal resolution was evaluated by scanning a plane target of holes and lines at the back of a lens of 2 cm focal length. For a beam diameter of 3 mm, when working at a line rate of 700 Hz, a transversal resolution better than 25 μm was achieved. For both cases presented below, the optics used determines a spot size smaller than 25 μm, however due to the way the carrier is created, the limitation of the bandwidth to 125 kHz and speckle effects, it is expected that the transversal resolution is worse than that of a confocal microscope using the same optics.

4. 3D images from the retina

In order to scan the retina, the output power was adjusted to 140 μW. The fan of scanned rays is brought to convergence at the eye pupil, as in all OCT reports on imaging the retina [2,3, 6,8]. An angular extent of $\pm 4.5^0$ in both planes X,Z and Y,Z was used (with an eye lens of ≈ 2 cm focal length this would give a transversal size of the image of ≈ 3 mm).

To illustrate the functionality of the system, 112 images have been collected in 56 seconds from the optic nerve of a volunteer at 700 Hz line rate and 2 frames a second, from a depth of 1.1 mm measured in air. We eliminated 12 images which registered blinks or large transversal movements. Dedicated software allows the reconstruction of the 3D image of the tissue volume to be seen from different angles, as illustrated in Fig. 2 and Fig. 3. The volume can be software orientated to any viewing angle and then can be explored along any of the axes X, Y or Z to show longitudinal slices in the planes (Y,Z) or (X,Z) or transversal slices in the (X,Y) plane respectively, as noted in Fig. 2. Identification of some of the layers in the optic nerve is shown in Fig. 3.

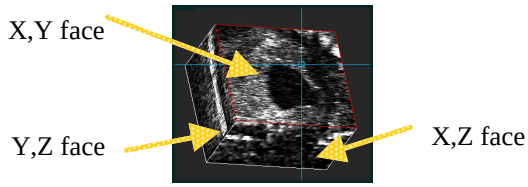

Fig. 2. (2.37 MB) Movie of three-dimensional in vivo optic nerve. The volume is explored from the retinal nerve fiber layer to the retinal pigment epithelium, along the optic axis. Volume size: 3 mm x 3 mm x 1.1 mm (air).

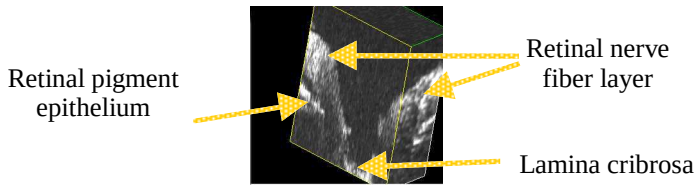

Fig. 3. (1.25 MB) (Y,Z) longitudinal slices in the stack of transversal OCT images from in vivo optic nerve at different X positions. Volume size: 3 mm x 3 mm x 1.1 mm (air).

The movie in Fig. 2 shows exploration of the 3D volume of the optic nerve of a volunteer along the Z axis (normal to the volunteer face) from the retinal nerve fiber layer to lamina

#23434 - $15.00 US Received September 03, 2000; Revised October 12, 2000

cribrosa. At the beginning, the retinal nerve fiber layer is shown. Then, blood vessels are visible, initially they appear bright, then the areas behind them become dark due to the high absorption of the light propagating through blood. The brightest layer by the end of the movie represents the retinal pigment epithelium. As we progress in depth, this very bright layer looks like a circle evolving from the periphery to the center, as consequence of the eye curvature. The last frame shows the lamina cribrosa, resolved again in the movie in Fig. 3, which shows longitudinal images of the optic nerve head. 3D volume rendering using SLO is presented in the reference [21], where the reasons for the importance of 3D visualisation of the optic nerve are also presented. However, our 3D rendering has more than 15 times better depth resolution due to the difference between the OCT and confocal principles. Clicking on different "faces" of the voxel volume, different cuts, transversal or longitudinal are made accessible.

5. 3D images from skin

Longitudinal OCT imaging has proved capable of differentiating coetaneous structures in skin [4,5]. We illustrate similar capability with measurements in vivo using our transversal OCT imaging instrument. The interface optics is modified to scan the ray parallel with the optic axis.

We collected images from the finger tip of a volunteer, placed at 3.5 cm away from the last lens of the interface optics. In order to increase the penetration depth, we reduced the scanning rate to 200 Hz a line and 1.75 s for a frame and increased the power to the skin to 0.27 mW. A glass window was used as support for the finger tip. 40 OCT transversal images were collected by moving the glass plate support along with the finger towards the OCT system in steps of 25 μm measured in air.

As shown by the movies in Fig. 4, 5, the finger-print ridges are visible touching the glass plate interface. The stratum corneum and the epidermis are clearly distinguishable.

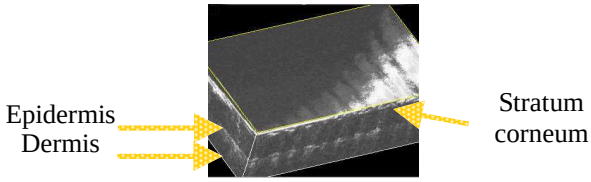

Fig. 4. (1.5 MB) Movie of three-dimensional in vivo finger tip. The volume is explored from the outside to the inside of the finger, along the optic axis. Volume size: 5 mm x 4 mm x 1 mm (air).

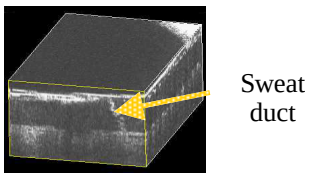

Fig. 5. (2.3 MB) (Y,Z) longitudinal slices in the stack of transversal OCT images from in vivo finger tip at different X positions. Volume size: 5 mm x 4 mm x 1 mm (air).

Transversal OCT images at different positions in depth in the finger tip are shown in the movie in Fig. 4. An en-face image of the epidermis is displayed for the first time (equivalent to peeling off the stratum corneum. On the sides of the reconstructed voxel profile, the longitudinal cuts from the current depth to larger depths are shown. The movie in Fig. 5 shows longitudinal (Y,Z) slices explored along the X axis. All the movies show different perspectives of the sweat ducts in the tissue. The transversal distribution of sweat ducts is clearly visible in the movie in Fig. 4 as a dotted pattern. The "scrolling through" feature of the 3D software allows the display of the entire duct in depth as shown by the movie in Fig. 5. The spiraled form of the sweat duct comes up very clearly in some of the frames. The two

#23434 - $15.00 US Received September 03, 2000; Revised October 12, 2000

movies together obviously ease the interpretation of the volume investigated, for instance the orientation, distribution and length of the sweat ducts is obtained only after corroborating the data from different orientations of the slices. The movies allow an easy association of the position of the ridges with the groves in the epidermis and they also show the tilted orientation of the glass plate.

6. Conclusions

3D volumes of the optic nerve and skin from the finger tip in vivo were generated using stacks of transversal OCT images collected from different depths. No averaging or enhancement procedures were performed. Although possible, we have not applied dynamic focus (maintainance in focus of the voxel sampled by coherence) as used in [11] due to the fact that in both cases illustrated in this paper, the depth of focus was larger than 1.5 mm and so larger than the range investigated in depth.

Our 3D presentation differs from that in [11], adapted to visualize the inner structure of translucent groups of cells and to rotate the 3D volume. We can also rotate the volumes in Fig. 2-5 and arrange them at different viewing angles (feature not animated in the paper).

The software program generating 3D profile is especially useful for a global investigation of the object by displaying an overall image of the volume scanned. As we have shown earlier [7,15] and as seen at the beginning of the movie in Fig. 2, the transversal OCT images look fragmented and are difficult to interpret (for instance when localised variations in surface height exceed the coherence length). Irrespective of their aspect when seen individually and irrespective of how fragmented they are, the final 3D rendering as shown here, offers the global view of the object.

Longitudinal OCT imaging of the retina has so far proved its capability to detect and image abnormalities such as diabetic retinopathy, the congenital pit of the optic nerve head, vitreous detachment, central serous chorioretinopathy, inflamatory optic neuropathy, macular holes and retinal pigment epithelium detachment [3, 22]. It is hoped that our system will enhance these capabilities even further by supplying a choice of image aspect which could be either transversal or longitudinal.

Obviously, such a system would avoid the necessity of gathering further data from the patient. The 3D volume generated as shown in the present paper gives the clinician access to slices of any orientation (for the time being plane, however circular slices can be software inferred along any contour defined in the transversal plane). Offering access to different angles of view as well as to orthogonal orientated slices will help image interpretation and improve the diagnostic.

The object movements (especially in the case of the eye), during the acquisition of each frame as well as between different frames, constitutes a major source of image blurring. This is especially visible when longitudinal cuts are generated from stacks of transversal OCT images. The value of the 3D presentation demonstrated in this paper is that the longitudinal cuts still show a very good resemblance to the hardware generated longitudinal OCT slices obtained by using either our method (Fig. 1 middle [7]) or conventional OCT imaging (Fig. 1 top). Work is under way to minimize the errors due to movements by software correcting procedures. Generally, a patient subject to such an investigation would require some training to stay still for the duration of image collection.

On the other hand, we have produced similar 3D movies as that in Fig. 2 and 3 by collecting only 40 transversal images which required an investigation time of only 20 seconds. The quality of such movies seems quite similar to that in Fig. 2 and 3, the only difference is in larger jumps in depth from slice to slice for the same range of depth investigated. We are also evaluating the quality of images collected at larger frame rates (we have recently achieved 1 kHz line rate and 5 Hz frame rate) with a corresponding reduction in the number of lines in the frame. All these issues are subject to a further report.

Acknowledgements: The authors acknowledge the support of the UK Engineering and Physical Sciences Research Council.

#23434 - $15.00 US Received September 03, 2000; Revised October 12, 2000